Rotational and Translational Dynamics of N-Butyl-N-methylpiperidinium Trifluoromethanesulfonimide Ionic Liquids Studied by NMR and MD Simulations

6 AUTHORS, INCLUDING:

Song Li
Huazhong University of Science and Technology
29 PUBLICATIONS   339 CITATIONS

SEE PROFILE

Gary A Baker
University of Missouri
246 PUBLICATIONS   8,820 CITATIONS

SEE PROFILE

Peter T Cummings
Vanderbilt University
518 PUBLICATIONS   11,688 CITATIONS

SEE PROFILE

Rotational and Translational Dynamics of *N*-Butyl-*N*-methylpiperidinium Trifluoromethanesulfonimide Ionic Liquids Studied by NMR and MD Simulations

Kee Sung Han,[†] Song Li,[‡] Edward W. Hagaman,*[,†] Gary A. Baker,[†,∥] Peter Cummings,[‡,§] and Sheng Dai[†]

[†]Chemical Sciences Division, Oak Ridge National Laboratory, Oak Ridge, Tennessee 37831, United States
[‡]Department of Chemical and Biomolecular Engineering, Vanderbilt University, Nashville, Tennessee 37235, United States
[§]Center for Nanophase Materials Science, Oak Ridge National Laboratory, Oak Ridge, Tennessee 37831, United States

S *Supporting Information*

ABSTRACT: Translational and rotational dynamics of the room temperature ionic liquid *N*-butyl-*N*-methylpiperidinium trifluoromethanesulfonimide, $[C_4mpip]$-$[Tf_2N]$, were investigated by ^1H, ^{19}F, and ^{13}C nuclear magnetic resonance (NMR) spectroscopy and molecular dynamics (MD) simulation. ^1H NMR and MD results for the temperature-dependent diffusion coefficients, D, spin−lattice relaxation times, T_1, and rotational correlation times, τ_c, for each site in the cation of $[C_4mpip][Tf_2N]$ are in good agreement. The T_1 data indicate a long N−CH$_3$ group rotation time, comparable to the overall molecular reorientation time. Correlation time comparisons between 1-butyl-3-methylimidizolium RTILs with different anions (Cl$^-$, PF$_6^-$, Tf$_2$N$^-$) argue against invoking hydrogen bond interactions between the N−CH$_3$ hydrogens and the electron rich center of the anion as an explanation of the long N−CH$_3$ rotation times. Correlation time comparisons between piperidinium and pyrrolidinium RTILs with a common anion (Tf$_2$N$^-$) suggest that correlation times for N−CH$_3$ rotation are primarily a function of the local structure of the cation.
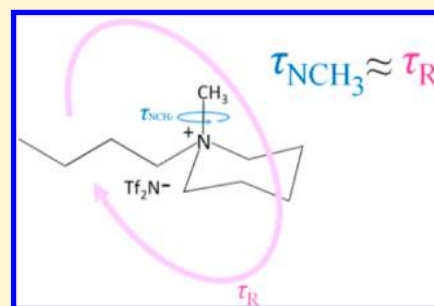
1. INTRODUCTION

Room temperature ionic liquids (RTILs) are solely composed of ions, the key feature that imbues RTILs with a unique suite of properties, *inter alia*, high ionic conductivity, thermal and chemical stability, nonflammability, and nonvolatility.[1] Changes in the structure of the cation or anion lead to significant variations in these properties. The rational design of new RTILs is essential for task-specific applications. The characterization of rotational and translational motion is important for designing and exploring the properties of new RTILs. Piperidinium-based RTILs have received attention due to their superior thermal and electrochemical stability, properties which are important in electrochemical devices such as lithium-ion batteries and supercapacitors.[2,3] The rotational and translational motion of various RTILs have been investigated by NMR spectroscopy[4−9] and classical MD simulations[5,10−12] to understand the relationship between macroscopic properties and the molecular or atomic level dynamics of the RTILs. In this work, the translational and rotational motions of *N*-butyl-*N*-methylpiperidinium trifluoromethanesulfonimde, $[C_4mpip][Tf_2N]$, were investigated by ^1H and ^{19}F pulsed field-gradient NMR (PFG-NMR) and ^1H and ^{13}C spin−lattice relaxation (T_1) measurements, respectively. MD simulations were performed to provide theoretical insight into the experimental dynamics measurements.

EXPERIMENTAL SECTION

Sample Preparation. $[C_4mpip][Tf_2N]$ was prepared by anion exchange of $[C_4mpip][Br]$ which was synthesized from the reaction of *N*-methyl piperidine with butyl bromide according to literature procedures.[2] Trace moisture was removed by heating the sample in the NMR tube at 80 °C under 0.5 Torr vacuum until the water signal was not detectable by NMR (1−2 days). Samples of 1-butyl-3-methylimidizolium trifluoromethanesulfonimide, $[C_4mim][Tf_2N]$, and *N*-butyl-*N*-methylpyrrolidinium trifluoromethanesulfonimide, $[C_4mpyr]$-$[Tf_2N]$, were synthesized by standard methods and dried under a vacuum to a water-free state prior to the NMR measurements. Samples of 1-butyl-3-methylimidizolium hexafluorophosphate, $[C_4mim][PF_6]$, and 1-butyl-3-methylimidizolium bromide, $[C_4mim][Br]$, were purchased from Sigma-Aldrich and dried before use.

NMR Experiments. NMR measurements were performed on a 9.4 T Bruker Avance NMR spectrometer at Larmor frequencies of 400.1, 376.4, and 100.6 MHz for ^1H, ^{19}F, and ^{13}C, respectively. Sample temperature was set with a Bruker BVT3000 temperature controller using a resistance heater in the probe, air for the heat transfer gas for high temperature, and N$_2$ gas evaporated directly from a liquid nitrogen dewar for low temperature. Sample temperatures were calibrated with 100%

ethylene glycol and 100% methanol for temperatures above and below 300 K, respectively, according to the Bruker temperature calibration manual. All spectra were acquired on neat liquids in an unlocked mode. T_1 was measured by the inversion recovery (180°-τ-90°-acquire) pulse sequence.[13]

Diffusion coefficients were measured using the stimulated echo bipolar pulse-gradient pulse (stebpgp) sequence. The gradient strength, g, was varied in 16 equal steps from 2 to 95% of the maximum gradient strength of the probe,[14] 54.4 ± 0.3 G/cm, determined by a ^{1}H magnetic resonance imaging method.[15] The data were fit to $S(g) = S(0) \exp[-D(\gamma\delta g)^2(\Delta - \delta/3)]$. In this equation, $S(g)$ and $S(0)$ are the echo heights at gradient g and 0, respectively, D is the diffusion coefficient, γ is the gyromagnetic ratio of nucleus investigated (^{1}H, ^{19}F, as appropriate), δ is the gradient-pulse length, and Δ is the duration between the two gradient pulses.[14] To eliminate sample convection effects induced by temperature gradients along the z (gradient) axis in measurements above 330 K, the sample height was restricted to 1 mm in a Microtube (Shigemi Inc., Japan). δ was fixed at 16 ms, and Δ was varied to optimize the decay of the echo height at maximum gradient strength.

The rotational correlation times, τ_c, at each resolved site of the cation of $[C_4mpip][Tf_2N]$ were calculated from ^{1}H and ^{13}C T_1 data, independently. The ^{1}H T_1 data were fit to the Bloembergen−Purcell−Pound (BPP) equation[16]

$$\frac{1}{T_1} = \frac{6}{5}\left(\frac{\mu_0}{4\pi}\right)^2 \frac{\gamma^4 \hbar^2}{b^6} I(I+1)$$
$$\times \left[\frac{\tau_c}{1+\omega_0{}^2\tau_c{}^2} + \frac{4\tau_c}{1+4\omega_0{}^2\tau_c{}^2}\right] \quad (1)$$

where γ is the gyromagnetic ratio of the proton (2.675×10^8 rad/T·s), $\hbar$ is reduced Planck's constant, b ($=\Sigma r$) is the distance between protons and the sum runs over all protons that are dipolar coupled to the proton evaluated, I is the nuclear spin number of the proton ($=1/2$), $\omega_0 = 2\pi\nu_0$, where ν_0 is the proton observe frequency (400.1 MHz at 9.4 T), and τ_c is the rotational correlation time. T_1's are determined as a function of temperature. Where a minimum in the T_1 vs T curve is observed, the relation $\omega_0\tau_c = 0.616$ is valid, τ_c is calculated as 2.45×10^{-10} s/rad, and the b term can be evaluated as the only unknown in eq 1.[16] The distance term is assumed constant as a function of temperature and used to calculate τ_c from T_1 data taken at different temperatures.

The ^{1}H−^{13}C dipole−dipole interaction is the dominant spin−lattice relaxation mechanism for ^{13}C nuclei directly bonded to hydrogen. The equation for spin−lattice relaxation by heteronuclear dipolar relaxation can be written as[7]

$$\frac{1}{T_1} = \frac{N}{10}\left(\frac{\mu_0}{4\pi}\right)^2 \frac{\gamma_H{}^2\gamma_C{}^2\hbar^2}{r^6}\left[\frac{\tau_c}{1+(\omega_H-\omega_C)^2\tau_c{}^2}\right.$$
$$\left. + \frac{3\tau_c}{1+\omega_C{}^2\tau_c{}^2} + \frac{6\tau_c}{1+(\omega_H-\omega_C)^2\tau_c{}^2}\right] \quad (2)$$

where N is the number of protons directly bonded to carbon, γ_H and γ_C are the gyromagnetic ratio of the proton and the carbon, respectively, r is the distance between the carbon and the proton, and ω_H and ω_C are the angular NMR frequencies of the proton and the carbon, respectively. For the ^{13}C nucleus ($I = 1/2$), $\gamma = 6.726 \times 10^7$ rad/T·s, and the observe frequency is $\nu_0 = \omega_0/2\pi = 100.6$ MHz at 9.4 T. The evaluation of τ_c from

^{13}C T_1 data using eq 2 does not require the observation of a T_1 minimum to evaluate the distance term, r, which is fixed at the nominal C−H bond distance (1.09 Å). Equation 2 incorporates the approximation that dipolar relaxation is determined through the directly attached protons ($N = 1$, 2, and 3 for CH, CH_2, and CH_3, respectively). Discrimination against next nearest neighbor protons relies on the inverse sixth power distance dependence of the dipolar interaction.

The measured correlation time monitored at the N−CH_3 resonance reflects contributions from molecular reorientation and rotation about the N−CH_3 bond. The N−CH_3 rotation rate, $1/\tau_{NCH_3}$, can be separated from the rate for molecular reorientation using the approximation $1/\tau_c \approx 1/\tau_R + 1/\tau_{NCH_3}$, where τ_c is the effective correlation time measured at the N−CH_3 site and τ_R is the overall molecular reorientation time given by τ_c of the ring carbons.[17] The correlation time plots (Figures 3b and 4b) show two values for the N−CH_3 resonances, τ_c from eq 1 or 2 (unfilled circles) and τ_{NCH_3} (filled circles). In this paper, τ_{NCH_3} specifically refers to the correlation time for rotation about the N−CH_3 bond derived through this approximation.

MD Simulation. All MD simulations were implemented with the Lucretius package using APPLE&P (Atomistic Polarizable Potential for Liquids, Electrolytes, & Polymers) force fields developed by Borodin,[11] in which polarizability terms were included. It has been reported that polarizable force fields predict the properties of molecules more accurately than nonpolarizable models.[18] The time step of 1 fs was used to integrate the equation of motion with a spherical cutoff of 10.5 Å in nonbonded van der Waals interactions. Long-range electrostatic interactions were treated using Ewald summation. A system consisting of 150 ion pairs was adopted at 1 atm. All bonds were constrained using the SHAKE method.[19] Periodic boundary conditions were applied in three dimensions. The system was equilibrated in the isothermal−isobaric (NPT) ensemble for 4 ns followed by 6−10 ns production runs at varying temperatures. Coordinates stored every 1 ps were used for the analysis.

The atomic diffusion coefficients were calculated at various temperatures with the Einstein relationship (3).

$$D = \lim_{t\to 0}\frac{1}{6t}\langle[r_i(t)-r_i(0)]^2\rangle \quad (3)$$

After linear fitting of the mean square displacement (MSD), the diffusion coefficient is obtained from the fitted slope divided by 6. The rotational autocorrelation functions (RACFs) are computed using the protocol of Borodin et al.[12] RACFs were computed with eq 4

$$P_l(t) = \langle\vec{e}(t)\cdot\vec{e}(0)\rangle \quad (4)$$

where $\vec{e}(0)$ is the initial unit vector lying along the C−H bond and $\vec{e}(t)$ is the same C−H unit vector at time t. The RACF is then fitted to the Kohlrausch−Williams−Watts (KWW) equation (eq 5),[12] yielding a curve. The rotational correlation time is then obtained as the integral from 0 to infinity of the fitted curve.

$$P_{KWW}(t) = A \exp\left[-\left(\frac{t}{\tau_{KWW}}\right)^\beta\right] \quad (5)$$

The apparent activation energy for translational and rotational motion was also computed.

■ RESULTS AND DISCUSSION

Diffusion Coefficient (D). The structures and numbering system of the molecules used in this work are collected in Scheme 1. The ^{1}H and ^{13}C NMR spectra of $[C_4mpip][Tf_2N]$

Scheme 1. Structure, Designation, and Numbering for Ionic Liquids

[C$_4$mpip][Tf$_2$N]   [C$_4$mpyr][Tf$_2$N]

[C$_4$mim][X]   X$^-$ = Cl$^-$, PF$_6^-$, Tf$_2$N$^-$ Tf$_2$N$^-$ = (CF$_3$SO$_2$)$_2$N$^-$
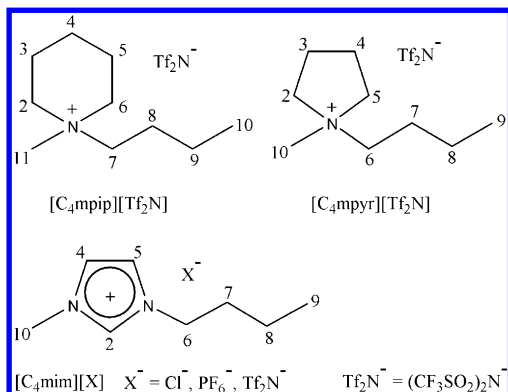
are presented in Figure 1a and b, respectively. Due to molecular symmetry, the resonances of H(2)/H(6), H(3)/H(5), C(2)/C(6), and C(3)/C(5) have equivalent chemical shifts.

The ^{1}H spectrum of the cation presents six resolved resonances. Each has been used independently to measure the diffusion coefficient, D, shown in the Arrhenius plot, Figure 2a. The average D is presented. The symbol used to indicate the data points is larger than the error bars representing one standard deviation. D of the anion obtained from monitoring the ^{19}F resonance is also plotted in this figure. The D values of $[C_4mpip]^+$ and $[Tf_2N]^-$ are nearly coincident over the temperature range, with the cation consistently showing a slightly greater D than the anion. Estimates of the hydrodynamic radius, r_s, for the ions from MD predict greater diffusivity for the anion, but these estimates do not account for the shape of the ions. The inset of Figure 2a shows the linear relationship of D with T/η predicted by the Stokes−Einstein theory of diffusion, i.e., $D = k_B T/6\pi\eta r_s$, where k_B is the Boltzmann constant, T is the absolute temperature, η is the

viscosity, and r_s is the hydrodynamic radius of the molecule. The Arrhenius plot of D is fit to the Vogel−Fulcher−Tamman (VFT) equation, $D = D_0 \exp[-B/(T - T_0)]$, where D_0, B, and T_0 are adjustable parameters which take the values 4.4 ($\pm$0.2) $\times$ 10^{-9} m^2/s, 654 $\pm$ 16 K, and 195 $\pm$ 1.5 K, respectively.

MD simulation results for cation diffusion are presented in Figure 2b and compared with the curve for the experimental data. The MD values are in good agreement with the magnitude of the experimental D's. The MD prediction does not capture the curvature in the Arrhenius plot, presenting a linear response with a slope matching that of the experimental data in the high temperature region. This difference may be caused by a combination of several factors, e.g., the APPLE&P force field used in this MD simulation and the time scale discrepancy between the NMR experiment and that for the simulation. The time scale for the NMR measurement is in the range of microseconds to milliseconds, while in the MD simulation the time length used for the MSD calculation is approximately 6 ns. However, the linear diffusive regime where the MSD increases linearly with time indicates that the simulation is sufficiently long enough to capture the magnitude of the diffusion coefficients. For ionic liquids in a glassy state encountered at low temperature, the force field is not suitable for predicting properties. The MD calculations are restricted to the high temperature region.

The activation energy, E_a, for translational diffusion for $[C_4mpip]^+$ was calculated from the Arrhenius equation, $D = D_0 \exp(-E_a/RT)$, where D_0 is the fitting parameter, R is the gas constant, and T is the absolute temperature. The E_a calculated from temperature dependent D obtained from ^{1}H PFG-NMR data is 33.8 $\pm$ 1.7 kJ/mol for T > 305 K and 54.0 $\pm$ 2.8 kJ/mol for T < 305 K. The latter value is similar to the larger E_a observed for 1,2-dimethyl-3-propylimidazolium trifluoromethanesulfonimide at low temperature.[7] The E_a calculated from the MD simulated D is 32.2 $\pm$ 1.3 kJ/mol, in good agreement with the E_a found in the high temperature region from the NMR measurement (see Figure 2b).

The translational correlation time for $[C_4mpip]^+$ can be calculated from D through the relation $\tau_{trans} = 2a^2/D$, where the radius, a, calculated from the MD volume, is 0.35 nm and $D = 4 \times 10^{-12}$ m^2/s at 300 K.[16] For $[C_4mpip]^+$, τ_{trans} is 60 ns, more than 2 orders of magnitude longer than the correlation times for molecular reorientation ($\approx$100 ps) where optimum overlap

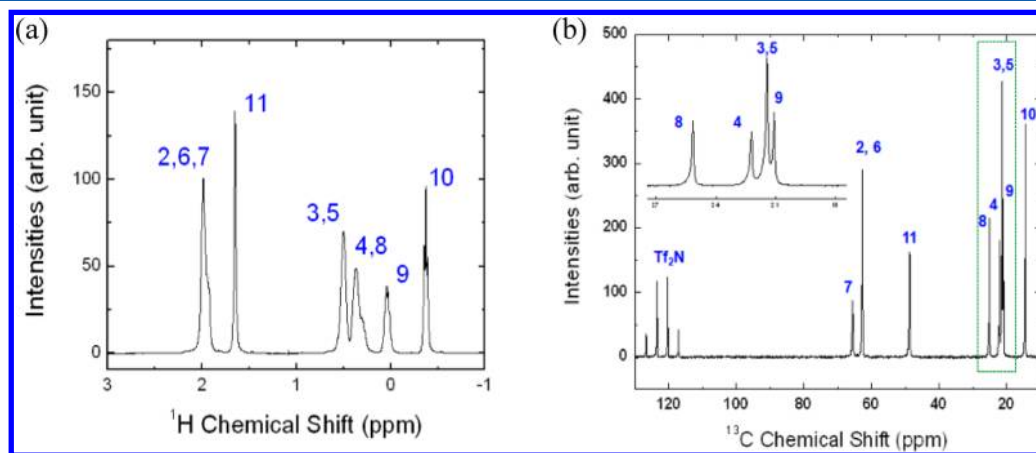**Figure 1.** (a) The ^{1}H NMR spectrum of $[C_4mpip][Tf_2N]$. (b) The ^{13}C NMR spectrum of $[C_4mpip][Tf_2N]$. The inset shows the boxed region in expanded form. The numbers on the resonances correspond to the positions identified on the structure.
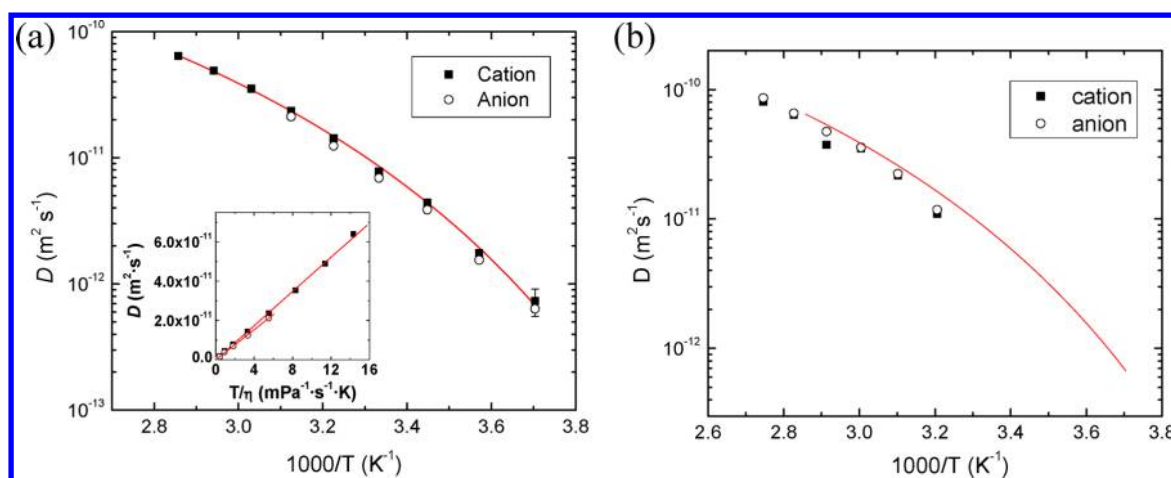
Figure 2. (a) Temperature dependent diffusion coefficient (D) of the cation, $[C_4mpip]^+$, and anion, $[Tf_2N]^-$, in $[C_4mpip][Tf_2N]$ measured by ^1H and ^{19}F PFG-NMR, respectively. The inset plots D of $[C_4mpip]$ and $[Tf_2N]$ in semilogarithmic scale as a function of T/η. Viscosity data are taken from the literature.[32] The fitted line in the main figure uses the VTF equation, $D = D_0 \exp(-B/T - T_0)$ (see text). (b) The MD simulated temperature dependence of D of the cation and anion of $[C_4mpip][Tf_2N]$. The fitted line from part (a) is superposed on the data for comparison.
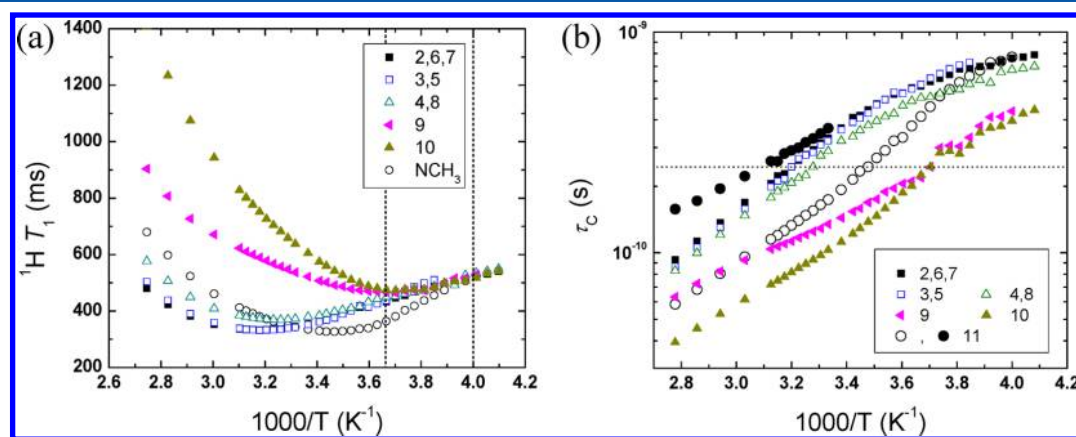

Figure 3. (a) ^1H T_1 temperature dependence of $[C_4mpip][Tf_2N]$. The vertical lines denote the crystallization (left) and melting (right) temperatures for $[C_4mpip][Tf_2N]$. (b) Rotational correlation times calculated from the temperature dependence of ^1H T_1 of $[C_4mpip][Tf_2N]$. The dotted line marks $\tau_c = 0.245$ ns, the time determined by the Larmor frequency of the protons in the NMR experiment performed at 9.4 T ($\omega_0\tau_c \approx 0.616$) at T_{1mim}. With our estimate of τ_{NCH_3}, the dipolar modulation frequency for $N-CH_3$ rotation (see text) is the slowest of any rotational motion, becoming equal to the Larmor frequency at the highest temperature.

between the NMR Larmor frequency and $1/\tau_c$ occurs ($\omega_0\tau_c \approx 1$). Consequently, dipolar fluctuation from translational motion is not an effective spin–lattice relaxation mechanism at the temperatures used in this work.

Rotational Correlation Time (τ_c). ^1H T_1. The temperature dependence of ^1H T_1 and τ_c for $[C_4mpip][Tf_2N]$ is shown in Figure 3a and b, respectively. The resonance bands, assigned in Figure 1a, show clear T_{1min} at temperatures higher than the melting point, T_m. The ^1H T_1 values for the ring sites, including H(7), average 0.35 ± 0.02 s (300 K), indicating the isotropic motion approximation for the ring is justified. T_1 values increase along the side chain toward the methyl terminus, a manifestation of increasing motion about sequential single bonds, i.e., segmental motion. From the T_1 of the ring protons (0.35 s), the $N-CH_3$ relaxation time for a *"static methyl group"*, i.e., a methyl group whose internal rotation rate is slow compared to overall molecular reorientation, is estimated to be 0.17 s.[20] Rapid internal motion can attenuate the dipolar coupling strength through a diminution in the spectral density function. For the specific case of a methyl group undergoing rapid internal rotation (relative to the molecular reorientation

time), the limiting reduction in the spin–lattice relaxation rate is $1/4$,[20,21] i.e., the T_1 is lengthened a factor of 4 over the value for a static methyl group. The T_1 for such a methyl group is expected to be 0.68 s at 300 K. The measured $N-CH_3$ T_1 of 0.34 s has a value between these limits, reflecting some degree of hindered rotational motion.

The correlation times derived from the T_1 data are shown in Figure 3b. Above room temperature, τ_c for the ring protons is linear with temperature. This is good evidence that a single motion dominates the relaxation of these protons. This motion is associated with overall molecular reorientation of the molecule. At low temperature, τ_c for the $N-CH_3$ resonance (unfilled circles) approaches τ_c for the ring resonances. From these correlation times, the $N-CH_3$ rotation time, τ_{NCH_3}, can be obtained (see the Experimental Section). The τ_{NCH_3} values, shown by the filled circles in the high temperature region, are marginally longer than the overall molecular reorientation time.

^{13}C T_1. The temperature dependence of ^{13}C T_1 and τ_c for $[C_4mpip][Tf_2N]$ is shown in Figure 4a and b, respectively. The T_1 values recorded at room temperature (300 K) are displayed
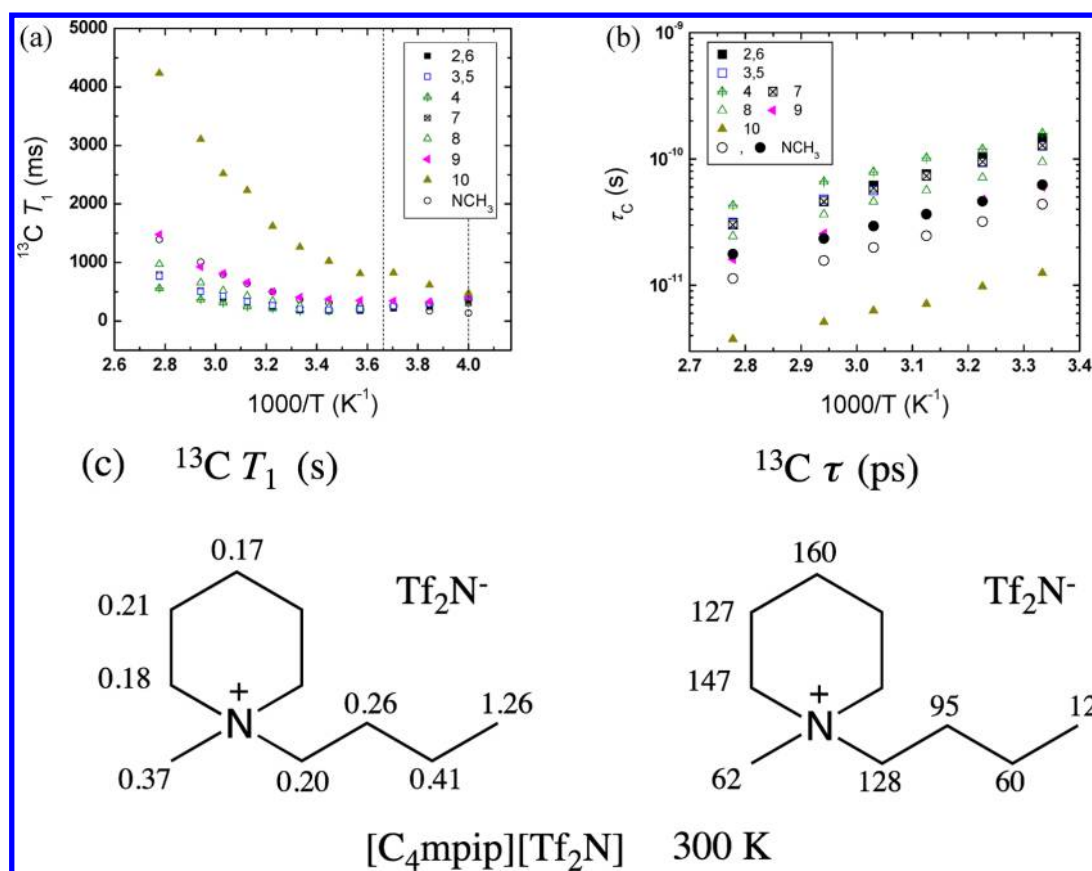
Figure 4. (a) ^{13}C T_1 temperature dependence of $[C_4mpip][Tf_2N]$. The dashed lines indicate the crystallization (left) and melting temperature (right). (b) Rotational correlation times, τ_C, calculated from the temperature dependence of T_1 of ^{13}C NMR in the high temperature region. (c) Summary of the ^{13}C T_1 (s) and τ_C (ps) values at room temperature (300 K). For N−CH$_3$, $\tau = \tau_{NCH_3}$.

on the structural formula (Figure 4c). The ring carbon T_1 values cluster in a tight group (0.19 ± 0.02 s) in apparent confirmation of the isotropic approximation.[22] T_1 values of the side chain carbons show the ordering expected for segmental motion, i.e., T_1 increasing monotonically along the chain toward the methyl end. This order is clearly demonstrated by the correlation times in Figure 4b. The chain end methyl, C(10), and the trifluoromethyl resonance of the anion (not shown) do not show a T_{1min} over the investigated temperature range. At 300 K, the N−CH$_3$ T_1 will vary between 0.13 s for a static methyl to 1.2 s for a rapidly rotating methyl ($\tau_{NCH_3} \ll \tau_c$).[22] The high temperature of the T_{1min} for the N−CH$_3$ resonance, similar to the ring sites, and its T_1 value (0.37 s) attest to the slow N−CH$_3$ rotation rate.

Correlation times are shown in Figure 4b for τ_c (unfilled circles) and τ_{NCH_3} (filled circles) for the N−CH$_3$ resonance. τ_{NCH_3} is marginally shorter than τ_c for the ring. Slow motional character of the N−CH$_3$ group is demonstrated in both the ^1H and ^{13}C data. Correlation times calculated from ^{13}C T_1 measurements are shorter than those from ^1H data, typically a factor of 2−4, but in some cases an order of magnitude. The discrepancy in the values has been pointed out previously, and possible reasons for this have been advanced.[23] Part of the difference arises from differences in actual C−H bond lengths and the bond length value of 1.09 Å used in the NMR estimate (eq 2). A 2−3% difference in the C−H bond length can generate a factor of 2 error in the correlation time calculated from ^{13}C T_1.[23] Correlation times from both ^1H and ^{13}C T_1 data,

plotted as a function of inverse temperature, are shown in Figures 2S−5S in the Supporting Information, where it is clear that the MD calculations align better with the ^1H data. The MD-generated τ_c's capture the trends of the experimental data well.

The correlation times of $[C_4mpip]^+$ in $[C_4mpip][Tf_2N]$, computed by MD simulation, are presented in Figure 5. The result shows the proton or carbon in the terminal methyl exhibits the shortest τ_c followed by those in N-methyl, alkyl chain, and the ring, i.e., the order observed in the NMR measurements. The short rotational correlation times of the
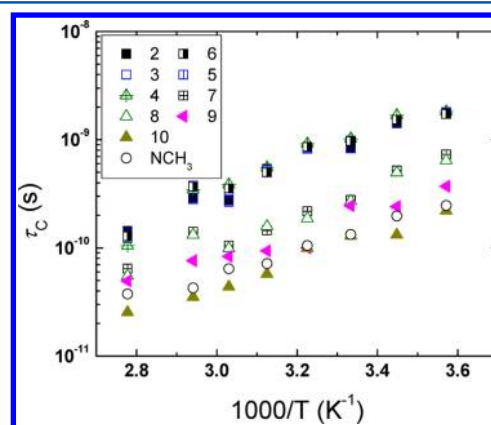

Figure 5. The rotational correlation times of $[C_4mpip][Tf_2N]$ as a function of temperature from MD simulations.

20783

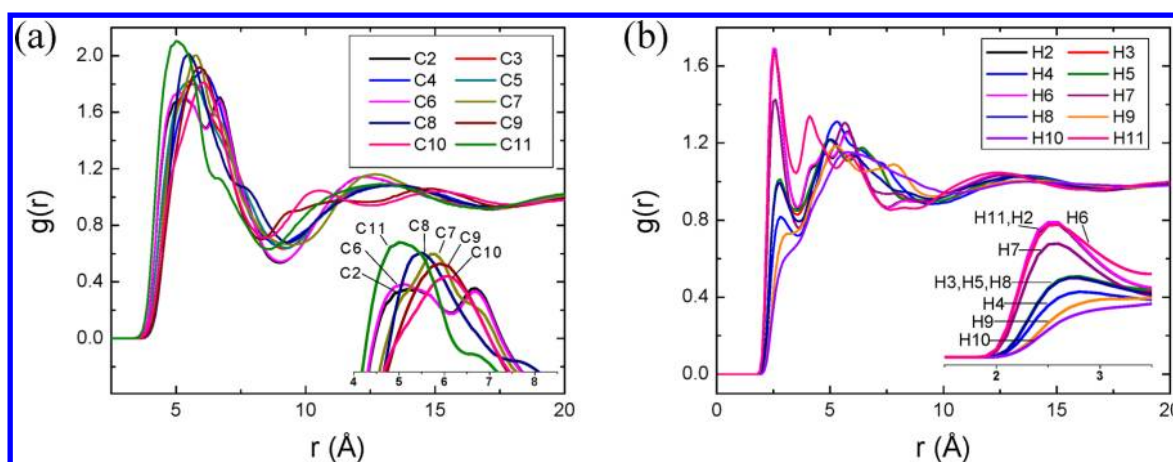dx.doi.org/10.1021/jp3069283 | *J. Phys. Chem. C* 2012, 116, 20779−20786

Figure 6. (a) Anion-carbon radial distribution functions (RDF) of $[C_4mpip][Tf_2N]$ at 300 K. (b) RDF of oxygen in the anion relative to hydrogen in the cation at 300 K.

side chain are the result of greater flexibility, i.e., increased degrees of motional freedom, of the side chain carbons compared to the ring.[8] Slower reorientation of the ring is explained by its larger inertial mass relative to the terminal carbon(s) of the side chain.

It has been noted that $N-CH_3$ rotation in imidazolium RTILs is slow, and arguments invoking hydrogen bond interactions have been advanced to rationalize these rates.[24,25] Evidence for the presence of hydrogen bonding is also obtained from the MD simulations. The strong electrostatic interaction between the piperidinium ring and the anion is shown by the ion−ion radial distribution function (RDF), $g(r)$, in Figure 6S (Supporting Information). The cation−anion RDF demonstrates that the cation−anion is closely packed due to electrostatic attraction compared to the relatively loosely packed cation−cation and anion−anion. To explore which part of the cation exhibits the strongest interaction with the anion, the RDFs of the center of mass of the anion relative to the individual carbons of the cation were computed (Figure 6a). The side chain terminal carbon C(10) has the lowest probability for close approach to the anion, attributed to its nonpolarity and long distance from the cation center. The N−CH_3 carbon is closest to the anion followed by the aminomethylene carbons of the piperidinium ring, C(2) and C(6). The high probability of the anion to interact with N-linked carbons (C(11), C(2) and C(6), C(7)), especially with the axial $N-CH_3$ group, is the consequence of the strong electrostatically driven approach of the ions. These carbons and their attached hydrogens are present at the interface of the ion pair by structural definition. The hydrogen bonds between O of the anion and H of the aminocarbon fragments are inferred from the RDFs of Figure 6b which exhibit shortest O−H distances of approximately 2.5 Å. O···H−C distances of this magnitude, and larger, that exceed the sum of the van der Waals O and H radii do not meet the criteria of the classical definition of the hydrogen bond but nevertheless fall within the modern, broad definition for weak hydrogen bonds.[26]

In contrast to the view that hydrogen bonding is causal to slow $N-CH_3$ rotation rates, the long τ_{NCH_3} may arise from the electronic and geometric structure inherent in the cation. This case is supported by the following experimental argument. If the $N-CH_3$ rotation rate is significantly slowed by specific interactions between the $N-CH_3$ protons and the heteroatoms of the anion, the $N-CH_3$ rotation rate should vary as a function of the anion. If the rotation rate is determined primarily by cation structure constraints, the rotation rates should be independent of the nature of the anion. This general argument is expected to be applicable to both imidazolium-based and tetraalkylammonium-based ILs containing $N-CH_3$ groups. In this work, we measured temperature dependent T_1's for $[C_4mim][Tf_2N]$ and use T_1 data from the literature for $[C_4mim][PF_6]$[24] and $[C_4mim][Br]$.[27] Since it is highly unlikely that anions as varied as Br^-, PF_6^-, and Tf_2N^- will have similar hydrogen bonding affinities, comparisons in this series should present a fair test if hydrogen bonding is important. Representative T_1 and τ_c data for $[C_4mim][Tf_2N]$ and $[C_4mim][PF_6]$ are shown in Figures 7S and 8S in the Supporting Information. Since these RTILs have different viscosities, the τ_{NCH_3} values are compared between RTILs which have the same overall molecular reorientation time. Experimentally, we use τ_c for C(2) to represent this value and compare the three RTILs at the temperature at which the C(2) τ_c is 100 ps. Since $\tau_c = 4\pi\eta a^3/3kT$,[16] this prescription holds η/T constant, and if the Debye radius, a, remains constant, i.e., if there is no specific association of the anion and cation, τ_{NCH_3} should be constant within the series. The τ_{NCH_3} value of the cation in combination with the $[Tf_2N]^-$, $[PF_6]^-$, and $[Br]^-$ anion is 14, 13, and 12 ps, respectively, i.e., 13 ± 1 ps. This variation, less than 10%, is comparable to the estimated error in the T_1 measurement. On this criterion, the slow $N-CH_3$ rotation rate is independent of the anion. Hydrogen bonding interactions with the $N-CH_3$ group must be associated with a low activation energy and short (≈ 1 ps) hydrogen bond lifetime in comparison to the $N-CH_3$ rotation correlation time of 10 ps. These two phenomena, $N-CH_3$ rotation and hydrogen bond formation, are not correlated. Any effect that might be ascribed to hydrogen bonding from the anion must be subtle, within the 10% error of the $N-CH_3$ rotation times.[28] Infrared spectroscopic evidence for the presence of hydrogen bonds in these ILs has been reported,[29,30] but the existence of long-lived hydrogen bonds is not supported by our data. The NMR criterion does not rule out weak hydrogen bond interactions.

Slow $N-CH_3$ rotation is observed in the tetraalkylammonium-based RTIL series.[31] Arguments invoking hydrogen bonds have been advanced to explain slow $N-CH_3$ rotation in $[C_4mpip][Tf_2N]$.[24] The τ_{NCH_3} values of $[C_4mpip][Tf_2N]$

and $[C_4mpyr][Tf_2N]$ allow us to compare rotation rates in structurally similar cations where the anion is kept constant. The ^{13}C T_1 data on which these comparisons depend are shown in Figure 4a and Figure 9S (Supporting Information), respectively. These cations are based on six-membered (piperidine) and five-membered (pyrrolidine) rings (Scheme 1) that will present significant differences in intramolecular steric interactions with substituents at the cation center. The first order prediction is that $N–CH_3$ rotation rates should be different if the controlling effect is intramolecular in origin. As above, the comparison is made with the ring τ_c set at 100 ps, i.e., at ca. 310 K for $[C_4mpip][Tf_2N]$ and 270 K for $[C_4mpyr][Tf_2N]$. τ_{NCH_3} of these RTILs differ by a factor of 3, 46, and 150 ps for $[C_4mpip]^+$ and $[C_4mpyr]^+$, respectively, demonstrating that $N–CH_3$ rotation rates are sensitive to cation structure.

CONCLUSION

Translational and rotational dynamics of $[C_4mpip][Tf_2N]$ were investigated by ^1H, ^{19}F, and ^{13}C nuclear magnetic resonance (NMR) spectroscopy and molecular dynamics (MD) simulations. The NMR T_1 data indicate slow internal $N–CH_3$ rotation rates, similar to overall molecular reorientation. MD simulations reproduce the trends seen in translational and rotational motion of $[C_4mpip][Tf_2N]$ and are in close agreement with the proton derived experimental correlation times. Correlation time comparisons in the imidazolium, piperidinium, and pyrrolidinium IL series indicate that long τ_{NCH_3} is primarily a function of cation structure. Hydrogen bond interactions between the $N–CH_3$ hydrogens of the cation and the oxygen atoms of the anion do not play a significant role in slowing $N–CH_3$ rotation rates. The long correlation time observed for $N–CH_3$ rotation may have its origin in the CN bond length, typically 4% shorter than aliphatic CC bond distances. This common structural feature explains the generality of the observation over an array of cation structures and hard and soft anions.

ASSOCIATED CONTENT

Supporting Information
Figures 1S–9S show (1) the temperature dependence of D for long and short sample lengths, (2–5) reorientational correlation time comparisons from ^1H, ^{13}C, and MD for each resolved site in $[C_4mpip]+$, (6) ion–ion center of mass distribution of $[C_4mpip][Tf_2N]$, (7, 8) temperature dependent ^{13}C T_1 and rotational correlation times of select sites in $[C_4mim][Tf_2N]$ and $[C_4mim][PF_6]$, respectively, and (9) temperature dependence of the ^{13}C T_1 and rotational correlation time of $[C_4mpyr][Tf_2N]$. This material is available free of charge via the Internet at http://pubs.acs.org.

AUTHOR INFORMATION

Present Address
∥Department of Chemistry, University of Missouri, Columbia, Missouri 65211, United States.

Notes
The authors declare no competing financial interest.

ACKNOWLEDGMENTS

REFERENCES

(1) Zhang, S.; Sun, N.; He, X.; Lu, X.; Zhang, X. *J. Phys. Chem. Ref. Data* **2006**, *35*, 1475−1517.
(2) Triolo, A.; Russina, O.; Fazio, B.; Appetecchi, G. B.; Carewska, M.; Passerini, S. *J. Chem. Phys.* **2009**, *130*, 164521.
(3) Ong, S. P.; Andreussi, O.; Wu, Y.; Marzari, N.; Ceder, G. *Chem. Mater.* **2011**, *23*, 2979−2986.
(4) Endo, T.; Imanari, M.; Seki, H.; Nishikawa, K. *J. Phys. Chem. A* **2011**, *115*, 2999−3005.
(5) Antony, J. H.; Mertens, D.; Dölle, A.; Wasserscheid, P.; Carper, W. R. *ChemPhysChem* **2003**, *4*, 588−594.
(6) Imanari, M.; Nakakoshi, M.; Seki, H.; Nishikawa, K. *Chem. Phys. Lett.* **2008**, *459*, 89−93.
(7) Hayamizu, K.; Tsuzuki, S.; Seki, S. *J. Phys. Chem. A* **2008**, *112*, 12027−12036.
(8) Hayamizu, K. *J. Chem. Phys.* **2010**, *133*, 194505.
(9) Imanari, M.; Uchida, K.-i.; Miyano, K.; Seki, H.; Nishikawa, K. *Phys. Chem. Chem. Phys.* **2010**, *12*, 2959−2967.
(10) Bedrov, D.; Borodin, O. *J. Phys. Chem. B* **2010**, *114*, 12802−12810.
(11) Borodin, O. *J. Phys. Chem. B* **2009**, *113*, 11463−11478.
(12) Borodin, O.; Gorecki, W.; Smith, G. D.; Armand, M. *J. Phys. Chem. B* **2010**, *114*, 6786−6798.
(13) Fukushima, E.; Roeder, S. B. W. *Experimental Pulse NMR: A Nuts and Bolts Approach*; Addision-Wesley Publishing Company: Reading, MA, 1981.
(14) Johnson, C. S., Jr. *Prog. Nucl. Magn. Reson. Spectrosc.* **1999**, *34*, 203−256.
(15) Yadav, N. N.; Torres, A. M.; Price, W. S. *J. Magn. Reson.* **2008**, *194*, 25−28.
(16) Abragam, A. *The Principles of Nuclear Magnetism*; Oxford University Press: New York, 1961.
(17) Allerhand, A.; Doddrell, D. *J. Am. Chem. Soc.* **1971**, *93*, 1558−1559.
(18) Halgren, T. A.; Damm, W. *Curr. Opin. Struct. Biol.* **2001**, *11*, 236−242.
(19) Ryckaert, J.-P.; Ciccotti, G.; Berendsen, H. J. C. *J. Comput. Phys.* **1977**, *23*, 327−341.
(20) Woessner, D. E. *J. Chem. Phys.* **1962**, *36*, 1−4.
(21) Antony, J. H.; Mertens, D.; Dolle, A.; Wasserscheid, P.; Carper, W. R. *ChemPhysChem* **2003**, *4*, 588−594.
(22) Allerhand, A.; Doddrell, D.; Komoroski, R. *J. Chem. Phys.* **1971**, *55*, 189−198.
(23) Dill, K.; Allerhand, A. *J. Am. Chem. Soc.* **1979**, *101*, 4376−4378.
(24) Carper, W. R.; Wahlbeck, P. G.; Antony, J. H.; Mertens, D.; Dolle, A.; Wasserscheid, P. *Anal. Bioanal. Chem.* **2004**, *378*, 1548−1554.
(25) Peppel, T.; Roth, C.; Fumino, K.; Paschek, D.; Kockerling, M.; Ludwig, R. *Angew. Chem., Int. Ed.* **2011**, *50*, 6661−6665.
(26) Desiraju, G. R.; Steiner, T. *The Weak Hydrogen Bond in Structural Chemistry and Biology*; Oxford: New York, 1999.
(27) Imanari, M.; Tsuchiya, H.; Seki, H.; Nishikawa, K.; Tashiro, M. *Magn. Reson. Chem.* **2009**, *47*, 67−70.
(28) Zhao, W.; Leroy, F. d. r.; Heggen, B.; Zahn, S.; Kirchner, B.; Balasubramanian, S.; Müller-Plathe, F. *J. Am. Chem. Soc.* **2009**, *131*, 15825−15833.
(29) Wulf, A.; Fumino, K.; Ludwig, R. *Angew. Chem., Int. Ed.* **2010**, *49*, 449−453.
(30) Dong, K.; Song, Y.; Liu, X.; Cheng, W.; Yao, X.; Zhang, S. *J. Phys. Chem. B* **2011**, *116*, 1007−1017.
(31) Guo, J.; Han, K. S.; Mahurin, S. M.; Baker, G. A.; Hillesheim, P. C.; Dai, S.; Hagaman, E. W.; Shaw, R. W. *J. Phys. Chem. B* **2012**, *116*, 7883−7890.

(32) Salminen, J.; Papaiconomou, N.; Kumar, R. A.; Lee, J.-M.; Kerr, J.; Newman, J.; Prausnitz, J. M. *Fluid Phase Equilib.* **2007**, *261*, 421−426.

20786

dx.doi.org/10.1021/jp3069283 | *J. Phys. Chem. C* 2012, 116, 20779−20786